Received October 28, 2021, accepted November 10, 2021, date of publication November 12, 2021,
date of current version November 22, 2021.

Digital Object Identifier 10.1109/ACCESS.2021.3127948

Exploring the Theoretical Limit of Voltage Transfer Ratio of Matrix Converter Under the Constraint of Rotating Vector

WEITAO DENG[1], (Member, IEEE), XIN FU[1], JIAYI TANG[1], WENWU XIE[1], AND BINGNAN JI[2]
[1]School of Information Science and Engineering, Hunan Institute of Science and Technology, Yueyang 414006, China
[2]EWEA-TECH Company Ltd., Zhengzhou 450000, China

Corresponding author: Bingnan Ji (jibn@yutong.com)

This work was supported in part by the Youth Project of Hunan Provincial Education Department under Grant 19B241, and in part by the Natural Science Foundation of Hunan Province under Grant 2020JJ4341.

ABSTRACT The rotating vectors of a matrix converter are uniquely featured by producing zero common-mode voltage, and control methods using them have the advantage of inherently achieving common-mode voltage minimization. However, the existing knowledge of their low voltage transfer ratio (VTR) has made it difficult for rotating vectors to get practical applications. This paper derives the theoretical limit of the VTR under the constraint of rotating vector. Firstly, the principle of selecting the voltage vector for maximum VTR is analyzed. Then the range of matrix converter input voltage phase angle is divided into intervals, and the phase angle of the selected rotating vector within each interval is determined. Finally, through integral and average calculations, the maximum VTR, $9/\pi^2$, is obtained, which is more than 80% higher than that of the linear modulation limit. Simulation and experiments are carried out to verify the correctness of the conclusion.

INDEX TERMS Voltage transfer ratio, matrix converter, rotating vector, permanent magnet synchronous motor.

I. INTRODUCTION

Matrix converter (MC)-fed permanent magnet synchronous motor (PMSM) system combines the advantages of MC, like compact structure, low harmonic pollution to the power grid, and those of PMSM, like high power density, good speed regulation performance, and is therefore widely used in high-performance motor control applications [1]–[3]. Among the state space vectors of the MC, rotating vectors (RVs) are characterized by continuous rotation and variation of distribution in the vector plane. In addition, RVs are inherently featured by producing zero common- mode voltage (CMV). Consequently, for the MC-fed motor system, employing the RVs to drive the motor is an excellent method of CMV suppression, which not only requires no adjustment of the hardware circuit structure, but also can achieve ideal suppression effect [4]–[7]. This idea has been realized in strategies like space vector modulation (SVM), direct torque control (DTC), etc., and has been verified effective in CMV minimization [8]–[18].

The associate editor coordinating the review of this manuscript and approving it for publication was Jinquan Xu.

However, due to the influence of the motion characteristic of the RV, the research of control strategies with RV is still in the preliminary stage. A significant factor that makes it difficult for rotating vectors to get practical applications is the existing knowledge of their low voltage transfer ratio (VTR). In [12], [13], it has been proved that when the RVs alone are used in SVM, the VTR cannot exceed 0.5 in the linear modulation area, which is severely lower than the maximum VTR of MC in the linear modulation area when all vectors are allowed to be used, i.e. 0.866. Overmodulation methods are usually employed in applications to achieve a higher VTR beyond the linear modulation area. Experiences show that the VTR can be increased by about 20% at most, i.e. from 0.866 to slightly higher than 1 [19], [20]. For RV -based methods, if an overmodulation strategy also achieve an increase of 20%, the VTR will ascend from 0.5 to around 0.6, which is still far from satisfactory. This presumption discourages the research of RV-based overmodulation strategies. As a result, no overmodulation strategy using RVs has ever been put forward up till now.

However, the above presumption, i.e., an increase of 20% in VTR by overmodulation, is actually not fit for the

TABLE 1. Space vectors of a 3 × 3 MC.

MC State	On Devices			V_o	θ_{Vo}	V_{com}
+1	S_{Aa}	S_{Bb}	S_{Cb}	$2/3u_{ab}$	0	$u_{bc}/3$
-1	S_{Ab}	S_{Ba}	S_{Ca}	$-2/3u_{ab}$	0	$u_{ac}/3$
+2	S_{Ab}	S_{Bc}	S_{Cc}	$2/3u_{bc}$	0	$u_{ca}/3$
-2	S_{Ac}	S_{Bb}	S_{Cb}	$-2/3u_{bc}$	0	$u_{ba}/3$
+3	S_{Ac}	S_{Ba}	S_{Ca}	$2/3u_{ca}$	0	$u_{ab}/3$
-3	S_{Aa}	S_{Bc}	S_{Cc}	$-2/3u_{ca}$	0	$u_{cb}/3$
+4	S_{Ab}	S_{Ba}	S_{Cb}	$2/3u_{ab}$	$2\pi/3$	$u_{bc}/3$
-4	S_{Aa}	S_{Bb}	S_{Ca}	$-2/3u_{ab}$	$2\pi/3$	$u_{ac}/3$
+5	S_{Ac}	S_{Bb}	S_{Cc}	$2/3u_{bc}$	$2\pi/3$	$u_{ca}/3$
-5	S_{Ab}	S_{Bc}	S_{Cb}	$-2/3u_{bc}$	$2\pi/3$	$u_{ba}/3$
+6	S_{Aa}	S_{Bc}	S_{Ca}	$2/3u_{ca}$	$2\pi/3$	$u_{ab}/3$
-6	S_{Ac}	S_{Ba}	S_{Cc}	$-2/3u_{ca}$	$2\pi/3$	$u_{cb}/3$
+7	S_{Ab}	S_{Bb}	S_{Ca}	$2/3u_{ab}$	$4\pi/3$	$u_{bc}/3$
-7	S_{Aa}	S_{Ba}	S_{Cb}	$-2/3u_{ab}$	$4\pi/3$	$u_{ac}/3$
+8	S_{Ac}	S_{Bc}	S_{Cb}	$2/3u_{bc}$	$4\pi/3$	$u_{ca}/3$
-8	S_{Ab}	S_{Bb}	S_{Cc}	$-2/3u_{bc}$	$4\pi/3$	$u_{ba}/3$
+9	S_{Aa}	S_{Ba}	S_{Cc}	$2/3u_{ca}$	$4\pi/3$	$u_{ab}/3$
-9	S_{Ac}	S_{Bc}	S_{Ca}	$-2/3u_{ca}$	$4\pi/3$	$u_{cb}/3$
+10	S_{Aa}	S_{Bb}	S_{Cc}	V_{in}	θ_{Vi}	0
-10	S_{Aa}	S_{Bc}	S_{Cb}	V_{in}	$-\theta_{Vi}$	0
+11	S_{Ab}	S_{Bc}	S_{Ca}	V_{in}	θ_{Vi} $-2\pi/3$	0
-11	S_{Ab}	S_{Ba}	S_{Cc}	V_{in}	$-\theta_{Vi}$ $+2\pi/3$	0
+12	S_{Ac}	S_{Ba}	S_{Cb}	V_{in}	θ_{Vi} $+2\pi/3$	0
-12	S_{Ac}	S_{Bb}	S_{Ca}	V_{in}	$-\theta_{Vi}$ $-2\pi/3$	0
$\mathbf{0_a}$	S_{Aa}	S_{Ba}	S_{Ca}	0	-	u_a
$\mathbf{0_b}$	S_{Ab}	S_{Bb}	S_{Cb}	0	-	u_b
$\mathbf{0_c}$	S_{Ac}	S_{Bc}	S_{Cc}	0	-	u_c

RV-based methods. In the linear modulation area of SVM, the synthesized output voltage vector is located within the inscribed circle of the vector polygon, and thus fails to take full advantage of the voltage vectors. As the shape of the polygon formed by the terminals of the RVs is variant with input voltage phase, the size of the inscribed circle is also variant, and the maximum VTR in linear modulation area is actually determined by the smallest inscribed circle. Consequently the RV-based SVM strategy achieves an even lower utilization of the voltage vectors in linear modulation area than expected. In other words, RV-based overmodulation methods can be expected to acquire a larger increase of VTR than around 20%. In fact, it has been deduced in [21] that the maximum VTR of RV-based DTC is much greater than 0.5; but the potential of voltage utilization is still not sufficiently

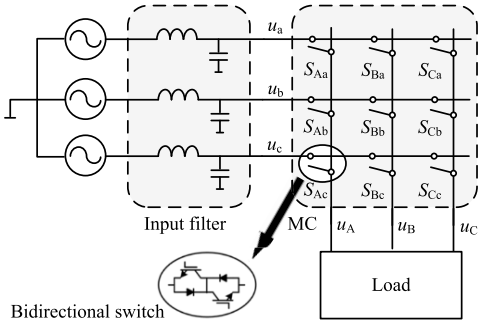

FIGURE 1. Circuit of matrix converter.

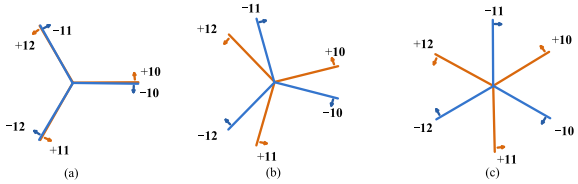

FIGURE 2. Distribution of rotating vectors. (a) $\theta_{Vi} = 0$. (b) $\theta_{Vi} = \pi/12$. (c) $\theta_{Vi} = \pi/6$.

achieved, as the selected RV has to meet the control requirement of flux magnitude in DTC.

In this paper, the principle of selecting the RV for maximum VTR is analyzed, and the theoretical limit of the VTR is calculated, which is higher than 0.9, indicating that RV-based overmodulation strategies can expect an increase of VTR by more than 80% compared with 0.5. Therefore, the research of RV-based overmodulation methods will be greatly encouraged, and rotating vectors will be applied more widely, exploiting their advantage of zero common-mode voltage to the full.

II. MATRIX CONVERTER

A 3 × 3 matrix converter connects each one of the 3 output terminals to each one of the 3 input terminals through 9 bidirectional switches, as shown in Fig. 1. A filter is used at the input of the MC to reduce the current harmonics. According to Fig. 1, the input and output voltages of the MC satisfy

$$\boldsymbol{u}_o = \begin{bmatrix} u_A \\ u_B \\ u_C \end{bmatrix} = \begin{bmatrix} s_{Aa} & s_{Ab} & s_{Ac} \\ s_{Ba} & s_{Bb} & s_{Bc} \\ s_{Ca} & s_{Cb} & s_{Cc} \end{bmatrix} \begin{bmatrix} u_a \\ u_b \\ u_c \end{bmatrix} = \boldsymbol{M} \cdot \boldsymbol{u}_i \quad (1)$$

where, $\boldsymbol{u}_i$ and $\boldsymbol{u}_o$ are input and output voltage vectors respectively, u_x ($x \in \{a, b, c, A, B, C\}$) is the phase voltage, s_{pq} ($p \in \{A, B, C\}$, $q \in \{a, b, c\}$) is the switching function of the bidirectional switch S_{pq} which connects the output phase p to the input phase q, $s_{pq} = 1$ represents the switch is on and $s_{pq} = 0$ represents it is off, $\boldsymbol{M}$ is the transfer matrix of the MC.

The switching state of the MC must satisfy the rules of avoiding short circuit at the input side of MC, as well as open circuit at the output side, due to the inductive characteristic of the load. Therefore there are 27 possible switching states, of which the corresponding output voltage vectors with their magnitude V_o and phase angle θ_{Vo} are listed in Table 1.

V_{in} and θ_{Vi} represent the magnitude and phase angle of input voltage vector. V_{com} represents the common mode voltage. The output voltage vectors corresponding to the switching states from $\pm\mathbf{1}$ to $\pm\mathbf{9}$ are referred to as active vectors, those corresponding to $\pm\mathbf{10}$ to $\pm\mathbf{12}$ are referred to as rotating vectors, and those corresponding to $\mathbf{0}_a$ to $\mathbf{0}_c$ are referred to as zero vectors.

The rotating vectors are featured by fixed amplitude and constantly changing phase angle. The phase angle of each RV varies periodically in accordance with θ_{Vi}, as shown in Table 1. Due to opposite rotating direction of the rotating vectors, their distribution is changing also with θ_{Vi}, and the angle between adjacent rotating vectors is variant between 0 and $2\pi/3$. Fig. 2(a) to Fig. 2(c) shows the instantaneous position of each RV when θ_{Vi} equals 0, $\pi/12$ and $\pi/6$, respectively.

III. MAXIMUM VTR OF MC WITH ROTATING VECTORS

Rotating vectors are employed in some control methods for MC-fed motor system to achieve CMV minimization. However, the existing RV-based methods cannot fully use the vector in each control step, which leads to low VTR. This paper proposes a method to reach the maximum VTR with rotating vectors.

A. PRINCIPLE OF VECTOR SELECTION FOR MAXIMUM VTR

Taking the direction of the stator flux linkage Ψ_s as the x-axis to establish an x-y rectangular coordinate system, the change rate of stator flux amplitude and the change rate of torque can be expressed as [3]

$$\mathrm{d}|\boldsymbol{\Psi}_s|/\mathrm{d}t = v_x \tag{2}$$

$$\mathrm{d}T_e/\mathrm{d}t = K_T\left(v_y - \omega_r|\boldsymbol{\Psi}_s|\right) \tag{3}$$

where v_x and v_y represent the x-axis and y-axis component of stator voltage respectively; ω_r is electrical angular speed of the rotor, and T_e is electromagnetic torque. K_T is related to the stator flux amplitude, the power angle, and motor parameters. At steady state, the rotor speed, the power angle and the stator flux amplitude can be approximately regarded as constant, i.e., $\omega_r|\boldsymbol{\Psi}_s|$ as well as K_T can be seen as a constant. It can be seen from (3) that the torque change rate is proportional to the difference between v_y and $\omega_r|\boldsymbol{\Psi}_s|$. Therefore, at any speed (in positive direction, for example), as long as the y-axis component of the employed voltage vector is larger than $\omega_r|\boldsymbol{\Psi}_s|$, the torque will always increase, so that the motor will accelerate. When the motor speed keeps unchanged even if the employed voltage vector has the largest y-axis component, it can be indicated that the motor has reached its maximum speed, and the converter outputs the maximum voltage with respect to the given input voltage. Therefore, **in order to reach the limit of VTR, the voltage vector with largest y-axis component should be employed in each control step.**

Within a control step, the selected output vector of a converter can be either a single voltage vector or a virtual vector equivalently synthesized by several voltage vectors (the sum of duty cycles being 1). For a matrix converter that uses only rotating vectors, the terminal of the equivalent output vector can be located at any point on the edge of the hexagon formed by the terminals of the six rotating vectors, or inside the hexagon as well. Obviously, no matter which direction is y-axis oriented, the terminal of the equivalent vector with largest y-axis component must be located on the edge of the hexagon, instead of inside it.

The shape of the hexagon formed by the six rotating vectors is varying with θ_{Vi}. As shown in Fig. 3, the dotted line hexagon is divided into six isosceles triangles by the six rotating vectors. Denote the three vertices of the triangle where y-axis is located as O, A and B (Point A and Point B are the terminals of the two adjacent rotating vectors), then the voltage vector with largest y-axis component is apparently located on the edge AB of the hexagon.

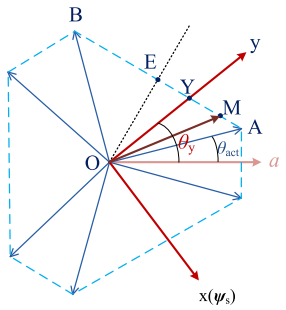

FIGURE 3. Diagram exploring the y-axis component of MC voltage vector.

Assume an arbitrary Point M on line segment AB, then

$$\overrightarrow{\mathrm{OM}} = \frac{1+m}{2}\overrightarrow{\mathrm{OA}} + \frac{1-m}{2}\overrightarrow{\mathrm{OB}} \tag{4}$$

where $m \in[-1, 1]$. Denote the intersection point of y-axis and line segment AB as Y, then

$$\overrightarrow{\mathrm{OY}} = \frac{1+y}{2}\overrightarrow{\mathrm{OA}} + \frac{1-y}{2}\overrightarrow{\mathrm{OB}} \tag{5}$$

where $y \in[-1, 1]$, then the y-axis component of $\overrightarrow{\mathrm{OM}}$ is

$$\overrightarrow{\mathrm{OM}}_y = \frac{\overrightarrow{\mathrm{OY}} \bullet \overrightarrow{\mathrm{OM}}}{||\overrightarrow{\mathrm{OY}}||} \tag{6}$$

As the denominator of (6) is irrelevant to m, substitute (4) and (5) into the numerator of (6), and denote the y-axis component of $\overrightarrow{\mathrm{OM}}$ as a function of m, i.e. $f(m)$, then

$$f(m) = \frac{V_{in}^2}{2||\overrightarrow{\mathrm{OY}}||}[(1-\cos\theta_{adj})ym + 1 + \cos\theta_{adj}] \tag{7}$$

where θ_{adj} is the angle between $\overrightarrow{\mathrm{OA}}$ and $\overrightarrow{\mathrm{OB}}$. According to (7), $f(m)$ is a linear function with respect to m. As 1-cosθ_{adj} is positive, when $y > 0$, the maximum value of $f(m)$ is always obtained at $m = 1$; when $y < 0$, the maximum value of $f(m)$ is always obtained at $m = -1$. In other words, the terminal of the voltage vector with the largest y-axis component is always located at point A or point B, not any other point on the line

segment AB. Therefore, **in order to achieve maximum VTR of MC with rotating vectors, virtual vectors are not in the scope of discussion; it is only necessary to select from the six rotating vectors a single one with the largest y-axis component in each control step**.

B. STRATEGY OF FINDING THE REQUIRED ROTATING VECTOR

To begin with, the value of the y-axis component of each RV is discussed respectively. Take +10 for an example, its projection on y-axis is

$$v_y(+10) = V_{in}\cos(\theta_{Vi} - \theta_y) \tag{8}$$

where θ_y is the angle of the positive y-axis referenced to phase a axis. According to (8), the curved surface of $v_y(+10)$ with respect to θ_{Vi} and θ_y both in the range of $(-\pi, \pi)$ is obtained with plotting tools, as shown in Fig. 4.

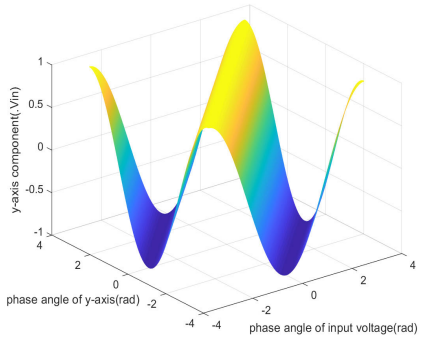

FIGURE 4. Y-axis component of +10 with respect to θ_{Vi} and θ_y.

Similarly, the curved surface of the y-axis component of the other five rotating vectors in the range of $\theta_{Vi} \in(-\pi, \pi)$ and $\theta_y \in (-\pi, \pi)$ can also be plotted, as shown in Fig. 5(a). According to the above analysis, the selected rotating vector in each control step is always the one with maximum y-axis component, therefore the curved surface of the y-axis component of the selected vector, i.e. v_y, is the upper enveloping surface of the figure in Fig. 5(a). This enveloping surface is separately shown in Fig. 5(b), and its top view is shown in Fig. 5(c). It can be seen from Fig. 5(c) that the range of θ_{Vi} and θ_y can both be evenly divided into 6 intervals, thus the whole plane of $2\pi \times 2\pi$ is divided into 36 sub-areas of $\pi/3 \times \pi/3$; v_y is the y-axis component of the same rotating vector within the same sub-area, and corresponds to different rotating vectors in adjacent sub-areas. By comparing the top view with the curved surface of the y-axis component of each rotating vector, it is not difficult to find out the rotating vector and its phase angle corresponding to v_y in different sub-areas. The value of the phase angle of the selected RV referenced to phase a axis, i.e. θ_{act}, is shown in Table 2.

To verify the correctness of Table 2, take the range of $\theta_{Vi} \in(0, \pi/3)$ and $\theta_y \in(0, \pi/3)$ for example. In this sub-area, $\sin(\pi/3 - \theta_{Vi}) > 0$, $\sin(\pi/3 - \theta_y) > 0$, thus the difference between the y-axis component of **+10** and **−11**, i.e. $v_y(+10) - v_y(-11)$, satisfies

$$\begin{aligned} &v_y(+10) - v_y(-11) \\ &\quad = V_{in}\cos(\theta_{Vi} - \theta_y) - V_{in}\cos(2\pi/3 - \theta_{Vi} - \theta_y) \\ &\quad = 2V_{in}\sin(\pi/3 - \theta_y)\sin(\pi/3 - \theta_{Vi}) > 0 \end{aligned} \tag{9}$$

Therefore, the y-axis component of **+10** is larger than that of **−11**. Similarly, it can be deduced that the y-axis component of **+10** is larger than that of any other rotating vector, and thus the rotating vector with largest y-axis component in the sub-area $\theta_{Vi} \in(0, \pi/3)$ & $\theta_y \in(0, \pi/3)$ is always **+10**, which is in accordance with Table 2. In the same way, it can be verified that the rotating vectors with largest y-axis component in other sub-areas are all in accordance with Table 2.

C. CALCULATION OF MAXIMUM VTR

According to the value of the phase angle θ_{act} of the rotating vector with largest y-axis component in different sub-areas, the average value of y-axis component of the selected rotating vector, $\bar{v}_y$, is

$$\begin{aligned} \bar{v}_y &= \frac{1}{2\pi}\int_{-\pi}^{\pi}\frac{1}{2\pi}\int_{-\pi}^{\pi} V_{in}\cos(\theta_{act} - \theta_y)\mathrm{d}\theta_y\mathrm{d}\theta_{Vi} \\ &= \frac{V_{in}}{4\pi^2}\sum_{k=0}^{5}\int_{-\pi+k\pi/3}^{-\pi+(k+1)\pi/3}\int_{-\pi}^{\pi}\cos(\theta_{act} - \theta_y)\mathrm{d}\theta_y\mathrm{d}\theta_{Vi} \\ &= \frac{V_{in}}{4\pi^2}\sum_{k=0}^{5}\int_{-\pi+k\pi/3}^{-\pi+(k+1)\pi/3}\sum_{h=0}^{5}\int_{-\pi+h\pi/3}^{-\pi+(h+1)\pi/3} \\ &\quad \times \cos(\theta_{act} - \theta_y)\mathrm{d}\theta_y\mathrm{d}\theta_{Vi} \\ &= \frac{V_{in}}{4\pi^2}\sum_{k=0}^{5}\sum_{h=0}^{5}\int_{-\pi+k\pi/3}^{-\pi+(k+1)\pi/3}\int_{-\pi+h\pi/3}^{-\pi+(h+1)\pi/3} \\ &\quad \times \cos(\theta_{act} - \theta_y)\mathrm{d}\theta_y\mathrm{d}\theta_{Vi} \end{aligned} \tag{10}$$

From Table 2, θ_{act} equals θ_{Vi} in the sub-area $\theta_{Vi} \in(0, \pi/3)$ & $\theta_y \in(0, \pi/3)$, thus

$$\begin{aligned} &\int_0^{\pi/3}\int_0^{\pi/3}\cos(\theta_{act} - \theta_y)\mathrm{d}\theta_y\mathrm{d}\theta_{Vi} \\ &\quad = \int_0^{\pi/3}\int_0^{\pi/3}\cos(\theta_{Vi} - \theta_y)\mathrm{d}\theta_y\mathrm{d}\theta_{Vi} \\ &\quad = \int_0^{\pi/3}(\sin(\pi/3 - \theta_{Vi}) + \sin\theta_{Vi})\mathrm{d}\theta_{Vi} = 1 \end{aligned} \tag{11}$$

Similarly, in each other sub-area, the integral result is also 1. Therefore

$$\bar{v}_y = \frac{V_{in}}{4\pi^2}\sum_{k=0}^{5}\sum_{h=0}^{5}1 = \frac{V_{in}}{4\pi^2}\cdot 36 = \frac{9V_{in}}{\pi^2} \tag{12}$$

Through similar calculations, it can be obtained that the x-axis component of the selected vector is 0. Thus the average amplitude of the output voltage vector is equal to $\bar{v}_y$, and accordingly the theoretical limit of VTR is

$$\bar{v}_y/V_{in} = 9/\pi^2 \approx 0.912 \tag{13}$$

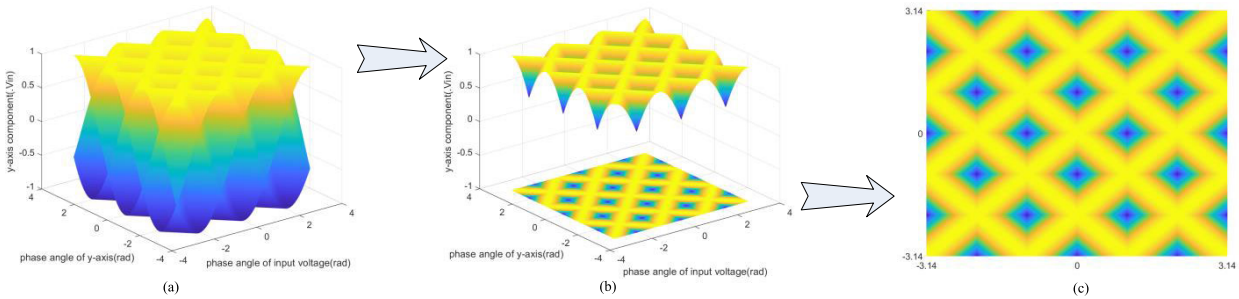

FIGURE 5. Y-axis component of RVs with respect to θ_{Vi} and θ_y. (a) 6 rotating vectors separately. (b) maximum y-axis component. (c) top view.

TABLE 2. Phase angle of the selected rotating vector.

θ_{Vi}		$(-\pi, -2\pi/3)$	$(-2\pi/3, -\pi/3)$	$(-\pi/3, 0)$	$(0, \pi/3)$	$(\pi/3, 2\pi/3)$	$(2\pi/3, \pi)$
θ_y	$(2\pi/3, \pi)$	$-\theta_{Vi}$	$\theta_{Vi}-2\pi/3$	$-\theta_{Vi}+2\pi/3$	$\theta_{Vi}+2\pi/3$	$-\theta_{Vi}-2\pi/3$	θ_{Vi}
	$(\pi/3, 2\pi/3)$	$\theta_{Vi}-2\pi/3$	$-\theta_{Vi}$	$\theta_{Vi}+2\pi/3$	$-\theta_{Vi}+2\pi/3$	θ_{Vi}	$-\theta_{Vi}-2\pi/3$
	$(0,\pi/3)$	$-\theta_{Vi}-2\pi/3$	$\theta_{Vi}+2\pi/3$	$-\theta_{Vi}$	θ_{Vi}	$-\theta_{Vi}+2\pi/3$	$\theta_{Vi}-2\pi/3$
	$(-\pi/3, 0)$	$\theta_{Vi}+2\pi/3$	$-\theta_{Vi}-2\pi/3$	θ_{Vi}	$-\theta_{Vi}$	$\theta_{Vi}-2\pi/3$	$-\theta_{Vi}+2\pi/3$
	$(-2\pi/3, -\pi/3)$	$-\theta_{Vi}+2\pi/3$	θ_{Vi}	$-\theta_{Vi}-2\pi/3$	$\theta_{Vi}-2\pi/3$	$-\theta_{Vi}$	$\theta_{Vi}+2\pi/3$
	$(-\pi, -2\pi/3)$	θ_{Vi}	$-\theta_{Vi}+2\pi/3$	$\theta_{Vi}-2\pi/3$	$-\theta_{Vi}-2\pi/3$	$\theta_{Vi}+2\pi/3$	$-\theta_{Vi}$

TABLE 3. Parameters of PMSM.

Number of pole pairs	p	4
Permanent magnet flux	Ψ_f	0.24Wb
Stator resistance	R_s	0.6Ω
Stator inductance	L_s	1.2mH
Rated power	P_N	1.6kW
Rated speed	n_N	1000r/min
Rated torque	T_N	15N·m
Rated frequency	f_N	66.7Hz

IV. SIMULATION AND EXPERIMENT

To verify the correctness of the theoretical limit of VTR, simulation and experiments are carried out on a MC-PMSM system. The parameters of the PMSM are listed in Table 3. The flowchart of the control algorithm is shown in Fig. 6.

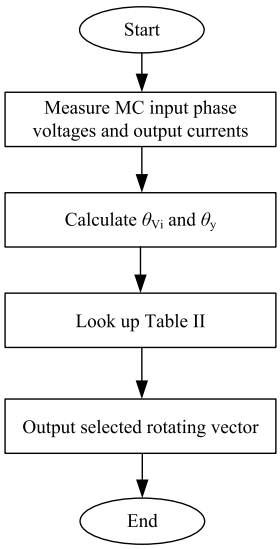

FIGURE 6. Flowchart of the proposed method.

A. SIMULATION

In the simulation, the input and output phase voltage waveforms at steady state are shown in Fig. 7(a), and their FFT results are shown in Fig. 7(b).

According to the fundamental amplitude of output voltage 36.5V and that of input voltage 40V, the VTR is accordingly 0.912, which agrees with the theoretically derived result.

B. EXPERIMENT

The MC-PMSM experiment setup is shown in Fig. 8. The MC control circuit is composed of a TMS320F28335 digital signal processor and an EP4CE6 FPGA. The program of the control algorithm runs in the DSP, and the program of a modulated four-step commutation of MC introduced in [15] runs in the FPGA.

In the experiment, the input and output phase voltage waveforms at steady state under no-load condition are shown in Fig. 9(a). Fig. 9(b) shows the FFT results of the input and output voltages. According to their fundamental amplitudes 34.1V and 30.5V, the VTR is accordingly 0.894.

Table 4 shows the measured output voltage and the calculated VTR results under different input voltage conditions. Due to unideal factors in the experiment, such as measurement error, the power switch voltage drop and the voltage drop over resistance caused by the neglected stator current,

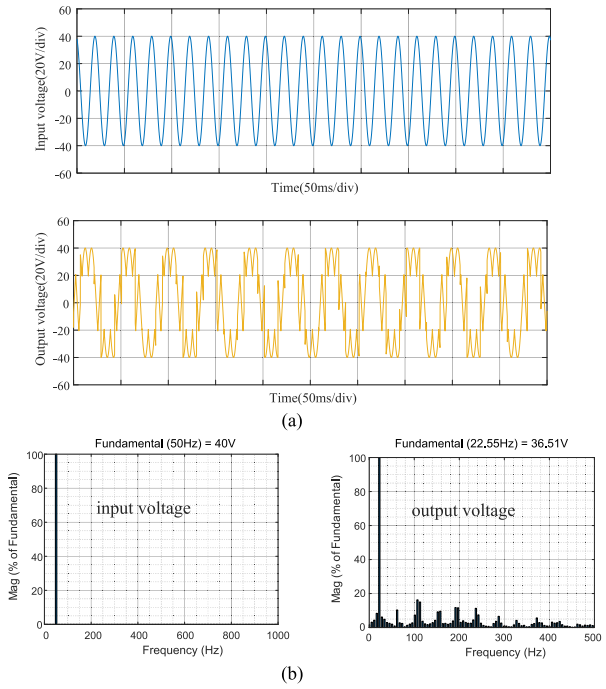

FIGURE 7. Simulation results (a) input and output voltage waveforms. (b) FFT results.

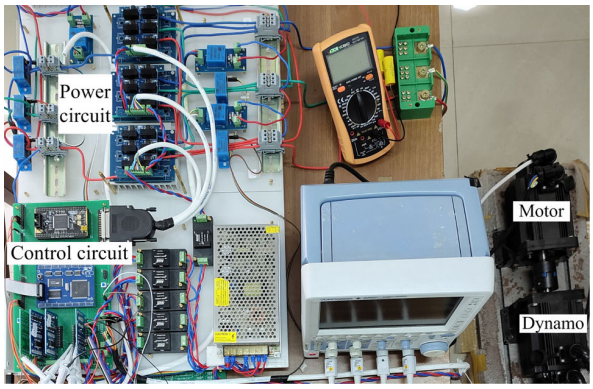

FIGURE 8. Experiment setup.

TABLE 4. Voltage transfer ratio results of the proposed method.

Input voltage (V)	Output voltage (V)	VTR	VTR error (%)
34.1	30.5	0.894	1.97
43.6	39.1	0.896	1.75
51.9	46.9	0.903	0.99
61.5	55.1	0.896	1.75

the actual VTR is slightly deviated from the theoretical value, but the experimental errors are all within acceptable range. The experimental results verify the correctness of the conclusion of this article.

For comparison, experiments under FOC at maximum linear modulation are also carried out. Fig. 10(a) shows the input and output phase voltage waveforms at steady state under no-load condition, and Fig. 10(b) shows the FFT results of

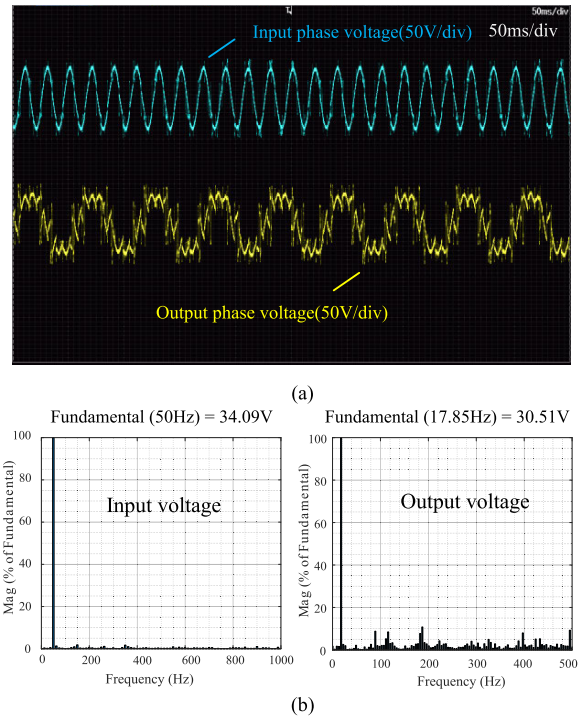

FIGURE 9. Experiment results of the proposed method(a) input and output voltage waveforms. (b) FFT results.

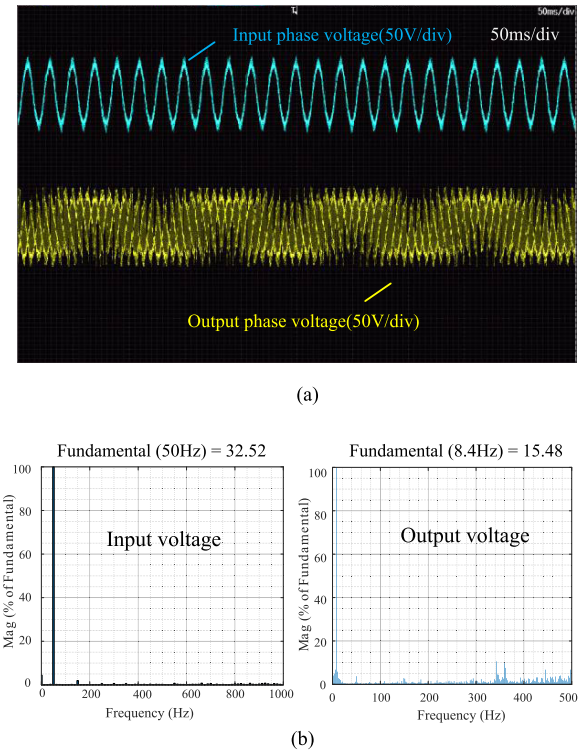

FIGURE 10. Experiment results of FOC under maximum linear modulation (a) input and output voltage waveforms. (b) FFT results.

the input and output voltages. According to their fundamental amplitudes 32.5V and 15.5V, the VTR is accordingly 0.477.

More experiments are carried out to calculate VTR under different input voltage conditions, and the results of both the

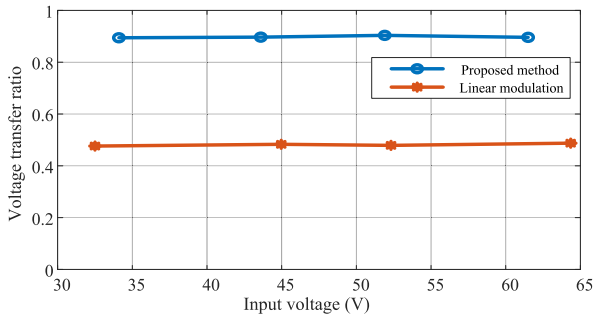

FIGURE 11. Voltage transfer ratio at different input voltage.

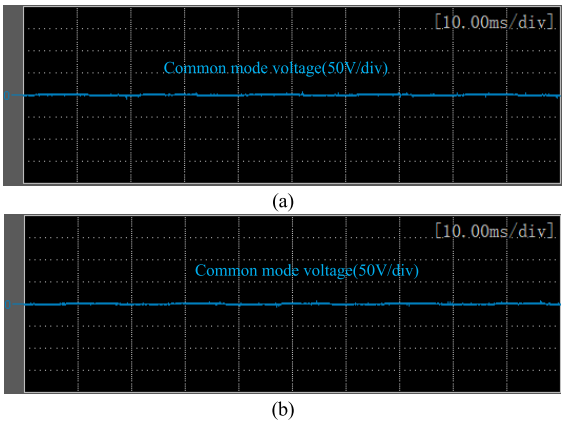

FIGURE 12. Common mode voltage. (a) proposed method. (b) FOC under maximum linear modulation.

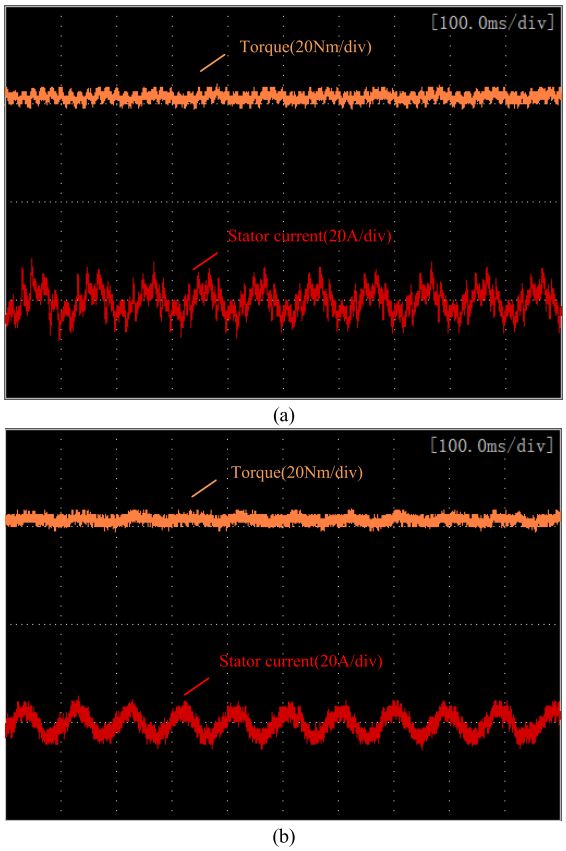

FIGURE 13. Torque and current. (a) proposed method. (b) FOC under maximum linear modulation.

TABLE 5. Steady state performance.

	Proposed method	Linear modulation
Torque ripple (Nm)	0.53	0.44
Current THD	78%	46%
Switching frequency(kHz)	0.176	3.1
VTR	0.894	0.477

proposed method and FOC at maximum linear modulation are shown in Fig. 11. It can be seen that the proposed method achieves a considerably higher VTR compared with linear modulation method, as indicated by this paper.

Fig. 12(a) shows the common mode voltage waveform of the proposed method, and Fig. 12(b) shows that of the FOC method under maximum linear modulation respectively. As both methods use only rotating vectors, common mode voltage are almost zero in both methods.

Fig. 13(a) shows the torque and stator current waveforms of the proposed method, and Fig. 13(b) shows that of the FOC method under maximum linear modulation. Torque ripple and current THD of both methods are listed in Table 5. In addition, average switching frequency of both methods are measured, and are also listed in Table 5.

It can be seen that the proposed method achieves significant increase in VTR compared with linear modulation method, at the sacrifice of evident increase of torque ripple and current THD. This is inevitable phenomenon, and is widely accepted in practicality. Meanwhile, as the proposed method achieves extremely lower switching frequency, and accordingly lower power loss, it is very fit for high-power and wide-speed regulation applications at high speed.

V. CONCLUSION

This paper proposes a method of calculating the maximum VTR of matrix converter using only rotating vectors, which is 0.912, and simultaneously provides a strategy for the matrix converter to reach it. Simulation and experiment research verified that the theoretical maximum VTR 0.912 can be reached with the proposed strategy, which is more than 80% greater than the maximum VTR of rotating vectors under linear modulation area. In addition, the proposed strategy achieves much lower switching frequency, and accordingly lower power loss, indicating its potential in high-power and wide-speed regulation applications at high speed. This paper reveals the theoretical limit of VTR with rotating vectors, and the conclusion will promote the research of RV-based modulation strategies, and provide support of further theoretical study and practical applications of RV-based control methods.

REFERENCES

[1] Z. Malekjamshidi, M. Jafari, J. Zhu, and D. Xiao, "Comparative analysis of input power factor control techniques in matrix converters based on model predictive and space vector control schemes," *IEEE Access*, vol. 7, pp. 139150–139160, 2019.
[2] S. Li, Z. Jin, X. Liu, X. Han, and W. Deng, "Open-current vector based SVM strategy of sparse matrix converter for common-mode voltage reduction," *IEEE Trans. Ind. Electron.*, vol. 68, no. 9, pp. 7757–7767, Sep. 2021.
[3] Y. Li, L. Qiu, Y. Zhi, G. Yan, J. Zhang, J. Ma, and Y. Fang, "An overmodulation strategy for matrix converter under unbalanced input voltages," *IEEE Access*, vol. 9, pp. 2345–2356, 2021.
[4] D. Han, C. T. Morris, and B. Sarlioglu, "Common-mode voltage cancellation in PWM motor drives with balanced inverter topology," *IEEE Trans. Ind. Electron.*, vol. 64, no. 4, pp. 2683–2688, Apr. 2017.
[5] Y. Xiang, X. Pei, M. Wang, P. Shi, and Y. Kang, "An improved H8 topology for common-mode voltage reduction," *IEEE Trans. Power Electron.*, vol. 34, no. 6, pp. 5352–5361, Jun. 2019.
[6] T. Shi, Q. Huang, Y. Yan, and C. Xia, "Suppression of common mode voltage for matrix converter based on improved double line voltage synthesis strategy," *IET Power Electron.*, vol. 7, no. 6, pp. 1384–1395, Jun. 2014.
[7] G. Zhang, H. Wang, Y. Yang, M. Su, C. Zhang, and F. Blaabjerg, "Common-mode voltage reduction with improved output voltage for three-to-five-phase indirect matrix converters," *IEEE J. Emerg. Sel. Topics Power Electron.*, vol. 8, no. 3, pp. 2918–2929, Sep. 2020.
[8] T. N. Mir, B. Singh, and A. H. Bhat, "FS-MPC-based speed sensorless control of matrix converter fed induction motor drive with zero common mode voltage," *IEEE Trans. Ind. Electron.*, vol. 68, no. 10, pp. 9185–9195, Oct. 2021, doi: 10.1109/TIE.2020.3020031.
[9] H.-N. Nguyen, M.-K. Nguyen, V.-Q.-B. Ngo, T.-T. Tran, J.-H. Choi, and Y.-C. Lim, "Input power factor compensation strategy for zero CMV-SVM method in matrix converters," *IEEE Access*, vol. 8, pp. 175805–175814, 2020.
[10] A. D. Arioni, T. S. Padilha, and S. V. G. Oliveira, "Expanded space vector modulation of direct matrix converters including hidden rotating pairs," *IEEE Trans. Ind. Electron.*, vol. 66, no. 11, pp. 8296–8307, Nov. 2019.
[11] H.-N. Nguyen and H.-H. Lee, "A modulation scheme for matrix converters with perfect zero common-mode voltage," *IEEE Trans. Power Electron.*, vol. 31, no. 8, pp. 5411–5422, Aug. 2016.
[12] H.-N. Nguyen and H.-H. Lee, "An enhanced SVM method to drive matrix converters for zero common-mode voltage," *IEEE Trans. Power Electron.*, vol. 30, no. 4, pp. 1788–1792, Apr. 2015.
[13] J. Lei, S. Feng, B. Zhou, H.-N. Nguyen, J. Zhao, and W. Chen, "A simple modulation scheme with zero common-mode voltage and improved efficiency for direct matrix converter-fed PMSM drives," *IEEE J. Emerg. Sel. Topics Power Electron.*, vol. 8, no. 4, pp. 3712–3722, Dec. 2020.
[14] T. N. Mir, B. Singh, and A. H. Bhat, "Delta-sigma modulation based common-mode voltage elimination in direct matrix converter," *IEEE Trans. Ind. Informat.*, vol. 17, no. 2, pp. 1048–1057, Feb. 2021.
[15] L. Wang, H. Dan, Y. Zhao, Q. Zhu, T. Peng, Y. Sun, and P. Wheeler, "A finite control set model predictive control method for matrix converter with zero common-mode voltage," *IEEE J. Emerg. Sel. Topics Power Electron.*, vol. 6, no. 1, pp. 327–338, Mar. 2018.
[16] W. Deng, H. Li, and J. Rong, "A novel direct torque control of matrix converter-fed PMSM drives using dynamic sector boundary for common-mode voltage minimization," *IEEE Trans. Ind. Electron.*, vol. 68, no. 1, pp. 70–80, Jan. 2021.
[17] W. Deng and S. Li, "Direct torque control of matrix converter-fed PMSM drives using multidimensional switching table for common-mode voltage minimization," *IEEE Trans. Power Electron.*, vol. 36, no. 1, pp. 683–690, Jan. 2021.
[18] W. Deng, X. Fu, and W. Xie, "Reduction of common-mode voltage in matrix convert-fed permanent magnet synchronous motor system with rotating vectors," *IEEE Access*, vol. 8, pp. 205894–205901, 2020.
[19] G. Zhang, J. Yang, Y. Sun, M. Su, Q. Zhu, and F. Blaabjerg, "A predictive-control-based over-modulation method for conventional matrix converters," *IEEE Trans. Power Electron.*, vol. 33, no. 4, pp. 3631–3643, Apr. 2018.
[20] B. Wang and G. Venkataramanan, "Six step modulation of matrix converter with increased voltage transfer ratio," in *Proc. 37th IEEE Power Electron. Spec. Conf.*, Jun. 2006, pp. 1–7.
[21] W. Deng, "Maximum voltage transfer ratio of matrix converter under DTC with rotating vectors," *IEEE Trans. Power Electron.*, vol. 36, no. 6, pp. 6137–6141, Jun. 2021.

WEITAO DENG (Member, IEEE) was born in Yueyang, China, in 1987. He received the B.S. and Ph.D. degrees in electrical engineering from Tianjin University, Tianjin, China, in 2010 and 2017, respectively.

He is currently a Lecturer with the School of Information Science and Engineering, Hunan Institute of Science and Technology, Hunan, China. His research interests include electric motor drives, power electronics, and their control systems.

XIN FU was born in Yueyang, China, in 1994. He received the B.S. degree in electrical engineering and its automation from the Hunan Institute of Science and Technology, Hunan, China, in 2019, where he is currently pursuing the master's degree with the School of Information Science and Engineering

His research interest includes AC motor control strategy.

JIAYI TANG was born in Yongzhou, China, in 2001. She is currently pursuing the B.S. degree in electrical engineering and its automation with the School of Information Science and Engineering, Hunan Institute of Science and Technology, Hunan, China. Her research interest includes AC motor control strategy.

WENWU XIE was born in Jingzhou, Hubei, China, in 1979. He received the B.S., M.S., and Ph.D. degrees in communication engineering from Huazhong Normal University, in 2004, 2007, and 2017, respectively.

From 2007 to 2009, he was a Communication Algorithm Engineer at Spreadtrum Communication Company Ltd. From 2012 to 2016, he was an Algorithm Manager at Mediatek Company Ltd. He is currently an Associate Professor with the Hunan Institute of Science and Technology. His research interests include communication algorithm and control algorithm.

BINGNAN JI was born in Anyang, China, in 1986. He received the Ph.D. degree in electrical engineering from Tianjin University, Tianjin, China, in 2015.

He is currently an Engineer with EWEA-TECH Company, Zhengzhou, China. His research interests include electric vehicles, power electronics, and their control systems.